Research in Mechanics of MEMS Devices

10 September 2000

Prepared by

D. J. CHANG, S. T. AMIMOTO, and A. D. BIRKITT
Space Materials Laboratory
Laboratory Operations

Prepared for

SPACE AND MISSILE SYSTEMS CENTER
AIR FORCE MATERIEL COMMAND
2430 E. El Segundo Boulevard
Los Angeles Air Force Base, CA 90245

Engineering and Technology Group

20000927 024

**THE AEROSPACE
CORPORATION**
El Segundo, California

This report has been reviewed by the Public Affairs Office (PAS) and is releasable to the National Technical Information Service (NTIS). At NTIS, it will be available to the general public, including foreign nationals.

This technical report has been reviewed and is approved for publication. Publication of this report does not constitute Air Force approval of the report's findings or conclusions. It is published only for the exchange and stimulation of ideas.

Michael Zambrana
SMC/AXE

REPORT DOCUMENTATION PAGE

1. AGENCY USE ONLY (*Leave blank*)	2. REPORT DATE 10 September 2000	3. REPORT TYPE AND DATES COVERED

4. TITLE AND SUBTITLE

Research in Mechanics of MEMS Devices

5. FUNDING NUMBERS

F04701-93-C-0094

6. AUTHOR(S)

D. J. Chang, S. T. Amimoto, and A. D. Birkitt

7. PERFORMING ORGANIZATION NAME(S) AND ADDRESS(ES)

The Aerospace Corporation
Laboratory Operations
El Segundo, CA 90245-4691

8. PERFORMING ORGANIZATION REPORT NUMBER

TR-99(8565)-3

9. SPONSORING/MONITORING AGENCY NAME(S) AND ADDRESS(ES)

Space and Missile Systems Center
Air Force Materiel Command
2430 E. El Segundo Boulevard
Los Angeles Air Force Base, CA 90245

10. SPONSORING/MONITORING AGENCY REPORT NUMBER

SMC-TR-00-28

11. SUPPLEMENTARY NOTES

12a. DISTRIBUTION/AVAILABILITY STATEMENT

Approved for public release; distribution unlimited

12b. DISTRIBUTION CODE

13. ABSTRACT (*Maximum 200 words*)

The objectives of the program are to investigate the validity of current solid mechanics principles for MEMS devices and to develop innovative experimental techniques for determining mechanical properties for MEMS elements. The task performed in FY98 was the study of Raman frequency shift of single-crystal silicon material under stresses using Raman spectroscopy. The study results, including development of the Eigenvalue equation for calculating the Raman frequency shift, experimental measurements on Raman frequencies for single-crystal silicon, and associated analyses, are presented in this report.

14. SUBJECT TERMS

MEMS, Stresses, Raman spectroscopy

15. NUMBER OF PAGES

21

16. PRICE CODE

17. SECURITY CLASSIFICATION OF REPORT UNCLASSIFIED	18. SECURITY CLASSIFICATION OF THIS PAGE UNCLASSIFIED	19. SECURITY CLASSIFICATION OF ABSTRACT UNCLASSIFIED	20. LIMITATION OF ABSTRACT

Contents

Figures

Tables

Executive Summary

This report documents the results of two tasks. The first task was the continued study of the Raman dynamic secular equation of cubic crystals, which relates the Raman frequency shifts and the surface stress field. The Raman frequency shifts under a general two-dimensional stress field were formulated. The second task was an experimental effort using Raman spectroscopy to measure the frequency shifts in a single-crystal structure that can be translated into surface stress fields.

In the first task, the three Raman frequency shifts under bi-axial stresses, τ_{11}, τ_{22}, and a shear stress τ_{12} in a local coordinate system for cubic crystal systems, were determined analytically. The relationship between the three Raman frequency-shift values and the three stress components is unique. Therefore, for a set of Raman frequency shifts, the three stress components will be uniquely determined.

In the second task, Ramon frequency shifts were measured using single-crystal silicon strips under uniaxial stress along either the (100) or the (110) orientation of the crystal system in a test fixture to test the derived expressions. The measured frequency shifts based on the calculated stresses agree well with the theory derived from the first task, thus validating the model.

1. Objective and Approaches

1.1 Objective

The objective of the work is to develop innovative experimental techniques for determining mechanical properties for MEMS elements. Specific tasks are:

(1) Derivation of relationships between Raman Shifts and applied two-dimensional surface stresses, and

(2) Development of innovative experimental techniques to determine mechanical properties important to MEMS components.

1.2 Approaches

For the duration of this program, two tasks were performed to achieve the objective. The tasks included an analytical evaluation of the Raman dynamic frequency equation and an experimental testing method to detect stresses under external loads applied primarily to single-crystal silicon strip specimens. The Raman dynamic frequency equation was examined in more detail, and the frequency shifts under general two-dimensional stress states were determined analytically. Because of the capability of the Raman technique in addressing very localized stress (spatial resolution 1–2 μm), potential stress non-uniformity can be identified. An observed stress non-uniformity in an otherwise theoretically uniform stress region will lead to a conclusion of material inhomogeneity. In turn, this understanding should lead to improved designs of MEMS devices using validated solid mechanics principles.

2. Introduction

The use of Raman spectroscopy is becoming known as a diagnostic in mapping stress in composites, semiconductors, and ceramics over the past few years and needs to be refined for space applications. For example, Raman has been used with some success to study relative stress at interconnects, near local oxidation structures, vias, and gate oxide structures, and to study adhesion effects between thin-film layers as affected by stress. The technique is also applicable to stress migration (SM) and electro-migration (EM) (two phenomena observed during life and reliability testing of interconnects) and therefore to circuit reliability.

Raman spectroscopy is a non-contact diagnostic technique. The Raman effect is observed as either the gain or loss of photon energy as a result of photon/phonon scattering from molecules or crystal lattices. The observed transitions are an indication of resonance in the vibrational energy of a material. As the material is strained, the energy state in the material is altered and thus the frequency is changed. The spatial resolution of Raman measurements can be made very high, on the order of 1 μm. It is very useful in detecting the surface stresses in either single-crystal or polycrystalline systems. The Raman spectroscopy technique is used here to demonstrate the detection of the residual stresses in a frequently used MEMS cantilever beam structure and in single-crystal test articles.

In this report, the Raman secular equation, which determines the Raman frequency shifts under an applied stress field, is first discussed. The experimental results on the Raman frequency shifts using various types of specimens and different stress fields are also discussed.

3. Raman Spectroscopy

3.1 Raman Secular Equation

The dynamic equations for the optical modes in diamond-like cubic crystals have the form[1,2]

$$m\ddot{u} = -\left[K_{ii}^{(0)} u_i + \sum_{klm} \frac{\partial K_{ik}}{\partial \eta_{lm}} \eta_{lm} u_k \right] \tag{1}$$

where u_i is the ith component of the relative displacement in the unit cell; m is the reduced mass of the atoms; $K_{ii}^{(0)} = m\,\omega_0^2$ is the effective spring constant in absence of strain; $(\partial K_{ik}/\partial \eta_{lm})\eta_{lm} = K_{iklm}\eta_{lm}$ is the change in the spring constant due to an applied strain η_{lm}; and i, k, l, and m refer to x, y, or z in an xyz coordinate system.

K_{iklm} are elements of a fourth-order tensor. They are the second derivatives of the potential energy with respect to the displacement fields u_i. Their magnitudes depend on the types of crystals. The crystal symmetry rules also apply to them. For a cubic crystal, for example, there are only three independent components, $K_{1111} = K_{2222} = K_{3333} = m\,p$, $K_{1122} = K_{1133} = K_{2233} = m\,q$, and $K_{1212} = K_{1313} = K_{2323} = m\,r$. Consequently, one obtains the following secular equation, whose solutions yield the frequencies of the optical phonons in the presence of strain. The constants p, q, and r are measured values for each type of crystal.

$$\begin{vmatrix} \left[p\varepsilon_{xx} + q(\varepsilon_{yy} + \varepsilon_{zz}) - \lambda \right] & 2r\varepsilon_{xy} & 2r\varepsilon_{xz} \\ 2r\varepsilon_{xy} & \left[p\varepsilon_{yy} + q(\varepsilon_{xx} + \varepsilon_{zz}) - \lambda \right] & 2r\varepsilon_{yz} \\ 2r\varepsilon_{xz} & 2r\varepsilon_{yz} & \left[p\varepsilon_{zz} + q(\varepsilon_{xx} + \varepsilon_{yy}) - \lambda \right] \end{vmatrix} = 0 \tag{2}$$

where the ε_{ij} are the strain components, and $\lambda = \Omega^2 - \omega_0^2$ represents the frequency shift. Since λ is so much smaller than ω_0, the shifted frequency Ω can be approximated by $\Omega = \omega_0 + \lambda/2\omega_0$ and $\Delta\Omega = \Omega - \omega_0 = \lambda/2\omega_0$.

It is seen from Eq. (2) that under an incident monochromatic light or laser, there will be up to three Raman frequency shifts. The shifts are a function of the elastic strains that are uniquely determined from the applied stresses. The shifts associated with some special stress states are discussed in the next section.

3.2 Frequency Shifts Associated With Two-Dimensional Stress Field and Examples

The strain components ε_{ij} are related to the stress components τ_{ij} by the following relationship:

$$\{\varepsilon\} = [S]\{\tau\} \tag{3}$$

where [S] is the compliance matrix. Its elements are components of a fourth-order tensor. For a material that is cubic such as silicon, the [S] has the following form:

$$[S]=\begin{bmatrix} S_{11} & S_{12} & S_{13} & 0 & 0 & 0 \\ S_{21} & S_{22} & S_{23} & 0 & 0 & 0 \\ S_{31} & S_{32} & S_{33} & 0 & 0 & 0 \\ 0 & 0 & 0 & S_{44} & 0 & 0 \\ 0 & 0 & 0 & 0 & S_{55} & 0 \\ 0 & 0 & 0 & 0 & 0 & S_{66} \end{bmatrix} \tag{4}$$

The Raman secular equation reduces to a cubic equation for λ for given values of elastic strains associated with the corresponding stress field. The solutions are designated as λ_1, λ_2, and λ_3.

The Raman frequency shifts associated with three different stress fields were analyzed; case 1 is a uniaxial stress field in the x-direction; case 2 is an equal biaxial stress field in the x- and y-directions; and case 3 is an equal tension and compression in the x and y-directions. Case 3 also corresponds to a pure shear stress field. Since Raman is a surface observation, the frequency shifts are only related to three stress components at the observed surface, one shear stress and two normal stress components. After solving Eq. (2), the unique frequency shifts associated with each case are shown in Table 1.

The Eigenvalues from Eq. (2) can be treated as a linear combination of the Eigenvalues of two decomposed stress fields for any given stress field, one associated with the hydrostatic stress field and the other associated with the deviatoric stress field. The hydrostatic and deviatoric stress fields are defined, respectively, as:

$$\{\tau_{ij}\}_h = \tau_0 = (\tau_{11} + \tau_{22} + \tau_{33})/3$$

$$\{\tau_{ij}\}_d = \tau_{ij} - \delta_{ij}\tau_0 \tag{5}$$

where δ_{ij} is the Knoecker's delta.

Using $\{\tau_{ij}\}_h$ and $\{\tau_{ij}\}_d$ as the stress fields, the corresponding strain fields are then computed. The three Eigenvalues for $\{\tau_{ij}\}_h$ are identical. The three Eigenvalues for $\{\tau_{ij}\}_d$ may be distinct. Let λ_h be

Table 1. Raman Frequency Shifts Corresponding to Various Limiting Stress Cases

	Frequency Shifts	
Case 1	$\Delta\Omega_1 = \tau_0(pS_{11}+2qS_{12})/2\omega_0$	$\Delta\Omega_2 = \Delta\Omega_3 = \tau_0[pS_{12}+q(S_{11}+S_{12})]/2\omega_0$
Case 2	$\Delta\Omega_1 = \Delta\Omega_2 = \tau_0[p(S_{11}+S_{12})$ $+q(S_{11}+3S_{12})]/2\omega_0$	$\Delta\Omega_3 = \tau_0[pS_{12}+q(S_{11}+S_{12})]/\omega_0$
Case 3	$\Delta\Omega_1 = \tau_0(p-q)(S_{11}-S_{12})/2\omega_0$ $\Delta\Omega_2 = -\tau_0(p-q)(S_{11}-S_{12})/2\omega_0$	$\Delta\Omega_3 = 0$

the Eigenvalue associated with $\{\tau_{ij}\}_h$, and let λ_{d1}, λ_{d2}, and λ_{d3} be the three Eigenvalues associated with $\{\tau_{ij}\}_d$.

By observation, we have

$$\lambda_h = (\lambda_1 + \lambda_2 + \lambda_3)/3$$

$$\lambda_{d1} = (\lambda_1 - \lambda_2)/3 + (\lambda_1 - \lambda_3)/3$$

$$\lambda_{d2} = (\lambda_2 - \lambda_1)/3 + (\lambda_2 - \lambda_3)/3$$

$$\lambda_{d3} = (\lambda_3 - \lambda_1)/3 + (\lambda_3 - \lambda_2)/3$$

or

$$\lambda_1 = \lambda_h + \lambda_{d1}$$

$$\lambda_2 = \lambda_h + \lambda_{d2}$$

$$\lambda_3 = \lambda_h + \lambda_{d3}$$

The frequency-shift values in terms of hydrostatic and deviatoric components are shown in Table 2. The frequency shifts are independent of the frequency of the incident light. It is seen that for an equal biaxial stress field, the frequency shifts under hydrostatic stress components are twice those of the uniaxial stress field. For the equal tension-compression case, there is no shift associated with the hydrostatic stress because it is zero. There are, however, two deviatoric stress-related shifts on either side of the reference frequency with the same magnitudes in frequency difference. The frequency shifts corresponding to a general stress field can be obtained numerically.

Table 2. Raman Frequency Shifts Corresponding to Hydrostatic and Deviatoric
Components

	Frequency shifts under hydrostatic stress components	Frequency shifts under deviatoric stress components
Case 1	$\Delta\Omega_h = \tau_o(p+2q)(S_{11}+2S_{12})/6\omega_o$	$\Delta\Omega_{d1} = \tau_o(p-q)(S_{11}-S_{12})/3\omega_o$
		$\Delta\Omega_{d2} = \Delta\Omega_{d3} = -\Delta\Omega_{d1}/2$
Case 2	$\Delta\Omega_h = \tau_o(p+2q)(S_{11}+2S_{12})/3\omega_o$	$\Delta\Omega_{d1} = \Delta\Omega_{d2} = \tau_o(p-q)(S_{11}-S_{12})/6\omega_o$
		$\Delta\Omega_{d3} = -2\Delta\Omega_{d1}$
Case 3	$\Delta\Omega_h = 0$	$\Delta\Omega_{d1} = \tau_o(p-q)(S_{11}-S_{12})/2\omega_o$
		$\Delta\Omega_{d2} = -\tau_o(p-q)(S_{11}-S_{12})/2\omega_o$
		$\Delta\Omega_{d3} = 0$

3.3 Frequency Shifts Associated With Two-Dimensional Stress Field

The two-dimensional stress field is appropriate to a surface where stress perpendicular to the surface is absent. This assumption applies to most surfaces. Consider this general two-dimensional stress field: τ_{11}, τ_{22}, and τ_{12} where τ_{11} and τ_{22} are normal stresses, and τ_{12} is the shear stress with respect to a Cartesian coordinate system with axes 1, 2, and 3. Further, let the 1, 2, and 3 axes coincide with the

7

principal axes of the cubic crystal material. If axis 3 does not coincide with the principal axis of the crystal, there will be six stress components present. This makes the analysis much more complicated.

Let the three stress components be related by the parameters α and β as follows:

$$\tau_{11} = \tau, \quad \tau_{22} = \alpha\, \tau, \quad \text{and} \quad \tau_{12} = \beta\, \tau \tag{6}$$

Eqs. (2), (4), and (5) combined with $\Delta\Omega = \Omega - \omega_o = \lambda/2\omega_o$ give the following three frequency shifts:

$$\Delta\Omega_1 = (\tau/4\omega_o)\{p(1+\alpha)(S_{11} + S_{12}) + q(1+\alpha)(S_{11} + 3S_{12}) + [(1-\alpha)^2(S_{11} - S_{12})^2(p-q)^2 + 4(rS_{44}\beta)^2]^{1/2}\},$$

$$\Delta\Omega_2 = (\tau/4\omega_o)\{p(1+\alpha)(S_{11} + S_{12}) + q(1+\alpha)(S_{11} + 3S_{12}) - [(1-\alpha)^2(S_{11} - S_{12})^2(p-q)^2 + 4(rS_{44}\beta)^2]^{1/2}\},$$

$$\Delta\Omega_3 = (\tau/2\omega_o)\{p(1+\alpha)S_{12} + q(1+\alpha)(S_{11} + S_{12})\} \tag{7}$$

The hydrostatic and deviatoric components of the frequency shifts can be expressed as:

$$\Delta\Omega_h = (\tau/6\omega_o)\{(p + 2q)(1+\alpha)(S_{11} + 2S_{12})\}$$

$$\Delta\Omega_{d1} = (\tau/12\omega_o)\{(p - q)(1+\alpha)(S_{11} - S_{12}) + 3[(p-q)^2(1-\alpha)^2(S_{11} - S_{12})^2 + 4(rS_{44}\beta)^2]^{1/2}\}$$

$$\Delta\Omega_{d2} = (\tau/12\omega_o)\{(p - q)(1+\alpha)(S_{11} - S_{12}) - 3[(p-q)^2(1-\alpha)^2(S_{11} - S_{12})^2 + 4(rS_{44}\beta)^2]^{1/2}\}$$

$$\Delta\Omega_{d3} = -(\tau/6\omega_o)\{(p - q)(1+\alpha)(S_{11} - S_{12})\} \tag{8}$$

The Eigenvectors associated with the three Eigenvalues $\lambda_1, \lambda_2,$ and λ_3 are

$$V_1 = \begin{bmatrix} 1 \\ -\Delta_1 \\ 0 \end{bmatrix} \frac{1}{\sqrt{1 + \Delta_1^2}}, \quad V_2 = \begin{bmatrix} -\Delta_2 \\ 1 \\ 0 \end{bmatrix} \frac{1}{\sqrt{1 + \Delta_2^2}}, \quad V_3 = \begin{bmatrix} 0 \\ 0 \\ 1 \end{bmatrix} \tag{9}$$

where

$$\Delta_1 = \frac{(1-\alpha)(S_{11} - S_{12})(p-q)/2 - D}{rS_{44}\beta}, \quad \Delta_2 = \frac{rS_{44}\beta}{(1-\alpha)(S_{11} - S_{12})(p-q)/2 + D},$$

$$D = \frac{1}{2}\sqrt{(1-\alpha)^2(S_{11} - S_{12})^2(p-q)^2 + 4(rS_{44}\beta)^2}$$

By observation, we note that $\Delta_1 = -\Delta_2$ and all three Eigenvectors are mutually orthogonal.

3.4   Selection Rule

The three frequency shifts associated with the stress field are not necessarily observable simultaneously at a specific orientation. Their detectability depends on the combination of the polarization of the incident light and scattered light. For cubic crystals such as silicon, the Raman tensors in the 1, 2, and 3 directions are

$$
R1 = \begin{bmatrix} 0 & 0 & 0 \\ 0 & 0 & d \\ 0 & d & 0 \end{bmatrix}, \qquad R2 = \begin{bmatrix} 0 & 0 & d \\ 0 & 0 & 0 \\ d & 0 & 0 \end{bmatrix}, \qquad R3 = \begin{bmatrix} 0 & d & 0 \\ d & 0 & 0 \\ 0 & 0 & 0 \end{bmatrix} \tag{10}
$$

The Raman tensors corresponding to three Eigenvectors are

$$
\overline{R}1 = \frac{1}{\sqrt{1+\Delta_1^2}} \begin{bmatrix} 0 & 0 & \Delta_1 d \\ 0 & 0 & d \\ \Delta_1 d & d & 0 \end{bmatrix}, \qquad \overline{R}2 = \frac{1}{\sqrt{1+\Delta_2^2}} \begin{bmatrix} 0 & 0 & d \\ 0 & 0 & \Delta_2 d \\ d & \Delta_2 d & 0 \end{bmatrix}, \qquad \overline{R}3 = \begin{bmatrix} 0 & d & 0 \\ d & 0 & 0 \\ 0 & 0 & 0 \end{bmatrix} \tag{11}
$$

where d is the lattice constant. Its magnitude is of the order of 10 nm.

Let e_i and e_s be the incident and scattered light with polarization of

$$
e_i^j = \begin{bmatrix} l_{i1}^j \\ l_{i2}^j \\ l_{i3}^j \end{bmatrix}, \qquad e_s^j = \begin{bmatrix} l_{s1}^j \\ l_{s2}^j \\ l_{s3}^j \end{bmatrix} \tag{12}
$$

where l_{km}^j are directional cosines, and $\left(l_{k1}^j\right)^2 + \left(l_{k2}^j\right)^2 + \left(l_{k3}^j\right)^2 = 1$, k = i,s, and j labels the frequency shifts, $\Delta\Omega_j$ in Eq. (7).

The scattering efficiency, I, is defined as $C\Sigma |e_i^j \ \overline{R}_j \ e_s^j|^2$ where C is a constant. Accordingly,

$$
I1 = C\,[l_{i3}^1 (l_{s1}^1 \Delta_1 + l_{s2}^1) d / \sqrt{1+\Delta_1^2}\,]^2,
$$

$$
I2 = C\,[l_{i3}^2 (l_{s1}^2 + l_{s2}^2 \Delta_2) d / \sqrt{1+\Delta_2^2}\,]^2, \tag{13}
$$

$$
I3 = C\,[(l_{i2}^3 l_{s1}^3 + l_{i1}^3 l_{s2}^3) d\,]^2
$$

9

It is seen from Eq. (13) that for the cases that correspond to backscattered light from the <001> surface, only z-polarized phonons can be observed. In addition, when the polarization angles of incident light and the scattered light are complements to each other, the expression $e_i^3 \overline{R}_3 e_s^3$ is maximized.

3.5 Determination of Stress Field with Known Raman Frequency Shifts

The existing literature on stress measurements using Raman spectroscopy has focused on Raman measurements or observation when the applied stresses are known for calibration purposes. Our challenge is the determination of a unique stress field τ_{11}, τ_{22}, and τ_{12} once the Raman frequency shifts are measured.

By examining Eq. (7) or (8), one finds that the three frequency-shift expressions are not linearly independent and hence cannot be used to uniquely determine the stress field. Therefore, one more equation is needed. In backscatter mode, one can select the incident and scattered polarization as

$$e_i = \begin{bmatrix} 0 \\ 0 \\ 1 \end{bmatrix}, \qquad e_s = \begin{bmatrix} 0 \\ 1 \\ 0 \end{bmatrix} \quad \text{and} \quad e_s = \begin{bmatrix} 1 \\ 0 \\ 0 \end{bmatrix} \tag{14}$$

Inserting these polarizations into Eq. (13), one obtains

$$I_1 = Cd^2/(1+\Delta_1^2), \qquad I_2 = C(\Delta_2 d)^2/(1+\Delta_2^2) \quad \text{using the first } e_s, \text{ and} \tag{15}$$

$$I_1 = C(\Delta_1 d)^2/(1+\Delta_1^2), \quad I_2 = Cd^2/(1+\Delta_2^2) \qquad \text{using the second } e_s. \tag{16}$$

By taking the ratio of I_1 and I_2 in Eq. (15) or (16), one obtains Δ_1 or Δ_2. α, β, and τ can then be determined from Eq. (7) as

$$\tau = \omega_o \left[\frac{\Delta\Omega_3}{pS_{12}+q(S_{11}+S_{12})} + \frac{(\Delta\Omega_1-\Delta\Omega_2)(1-\Delta_1^2)}{(S_{11}-S_{12})(p-q)(1+\Delta_1^2)} \right],$$

$$\alpha = 1 - \frac{(\Delta\Omega_1-\Delta\Omega_2)(1-\Delta_1^2)(2\omega_o)}{(S_{11}-S_{12})(p-q)(1+\Delta_1^2)\tau} \tag{17}$$

$$\beta = -\frac{(1-\alpha)(S_{11}-S_{12})(p-q)\Delta_1}{(1-\Delta_1^2)rS_{44}}$$

It is noted that the same information can be obtained by using either the first e_s or the second e_s with $\Delta_2 = -\Delta_1$. Also, The following limits of Δ_1 and Δ_2 exist:

$$
\begin{aligned}
&\Delta_1, \Delta_2 \in (-1,1), && \beta \in (-\infty, \infty) \\
&\text{As } \beta \to -\infty, && \Delta_1 \to -1, && \Delta_2 \to +1 \\
&\text{As } \beta \to \infty, && \Delta_1 \to +1, && \Delta_2 \to -1 \\
&\text{At } \beta = 0, && \Delta_1 = \Delta_2 = 0
\end{aligned}
\tag{18}
$$

A plot of Δ_2 versus β for values of $\alpha = -1, -0.5, 0, 0.5,$ and 1.0 is depicted in Figure 1. Also, the analysis has shown that for $|\beta|$ greater than 1, the sensitivity becomes poor for a given value of α.
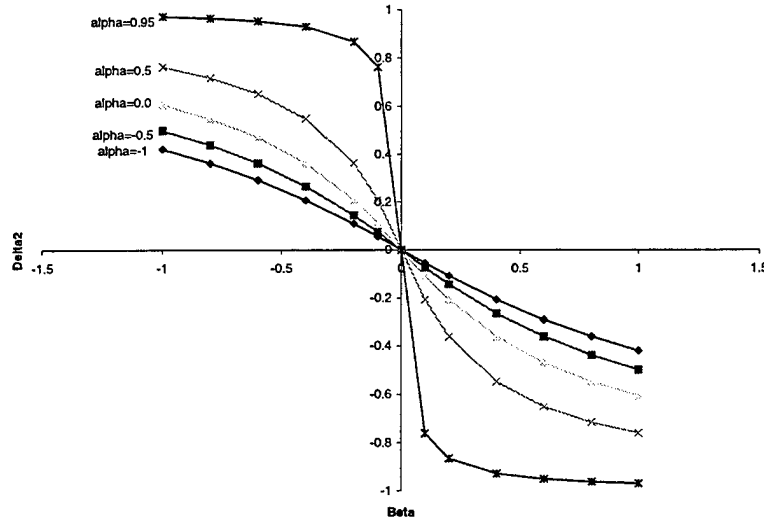

Figure 1.   Plot of β versus Δ_2 for single-crystal silicon ($\alpha = -1, -0.5, 0, 0.5, 0.95$).

11

4. Raman Stress Experimental Setup and Measurements

4.1   Specimen Description

Experimental test calibration specimens were made of single-crystal silicon. The specimen was in a strip configuration. The strip specimen was clamped into the holder at its two end regions. The specimen, with a clear span, L, of 5.72 cm (2.25 in.), was loaded with two rollers that are 1.91 cm (0.75 in.) apart and are located symmetrically with respect to the center of the specimen. Loads in the samples were induced by turning a set screw located along the centerline of the strip. The magnitudes of the loads were recorded through the output of a load cell located at the tip of the load screw. The maximum stress for the strip is

$$\sigma_s = 3Pb^2/(Lwt^2) \tag{19}$$

where P is the total load measured by the load cell, b and L are the dimensions shown in Figure 2, and w and t are the width and thickness, respectively, of the strip.

Single-crystal silicon (Si) strip samples normal to the <001> plane were fabricated. The sample dimensions were 12.7 mm (0.500 in.) wide and 0.394 mm (0.0155 in.) thick. They consist of two types such that a unidirectional stress could be applied either in the (110) or (100) crystal directions.

4.2   Test Apparatus

In the Raman stress experimental setup, a monochromatic light or laser shines through a microscope onto the surface of a specimen. The specimen sits on a translation stage whose motion is controlled by a micrometer. The spectrometer output is the intensity of the Raman signal as a function of frequency. A reference spectrum is taken for an unstressed sample. When the specimen is placed in a stressed state, the spectrum will show a frequency shift, which is linear to the applied stress. A Ne penray lamp was used for calibration lines to reliably and accurately measure the silicon transition.

The measurements were conducted using an argon laser line (wavelength 488 nm). The amount of frequency shift depends upon the stress state and can be determined from Eq. (2). The diameter of
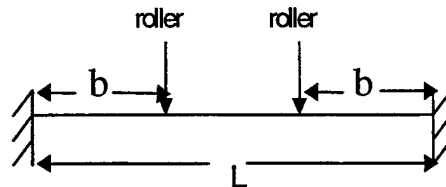
Figure 2. Schematics of strip specimen.

13

the laser spot is typically 1 to 2 μm. Therefore, a stress variation can be mapped out accurately. Raman spectra were acquired in integration mode using 10 scans at 2 s per scan.

4.3　Results

Figure 3 depicts the Raman spectra of a wafer cut from an annealed single-silicon crystal boule. The spectra were curve fit using a least-squares fitting procedure. In general, the fitting error was on the order of 0.005 cm^{-1} and is too small to be considered significant. The measured average center location wave number is 520.28 cm^{-1} with an uncertainty of 0.06 cm^{-1}. This uncertainty corresponds to an equal biaxial stress of $\pm$14.7 MPa ($\pm$2.1 ksi), which indicates the resolution of the technique. Measurements were also taken on an annealed polysilicon layer deposited on a SiO$_2$ layer on top of a single-crystal silicon substrate (see Figure 4). These measurements showed a spatial variability of $\pm$38.6 MPa ($\pm$5.6 ksi), well in excess of the measurement resolution, indicating the presence of residual stress..

A calculation was made based on the p, q, r, and elastic constants of single-crystal silicon[1]. For single crystal silicon, p =-1.43 x 10^{28}(s^{-2}), q = -1.89 x 10^{28}(s^{-2}), and r = -0.59 x 10^{28}(s^{-2}). The calculated results also show the Raman shifts in cm^{-1} as follows:

For uniaxial stress, σ:　　　$\Delta\Omega_1 = 7.83 \times 10^{-11}\sigma$ and $\Delta\Omega_2 = \Delta\Omega_3 = 2.00 \times 10^{-10}\sigma$.

For equal biaxial stress, σ:　　$\Delta\Omega_1 = \Delta\Omega_2 = 2.79 \times 10^{-11}\sigma$ and $\Delta\Omega_3 = 4.00 \times 10^{-10}\sigma$,

where σ is in dyne/cm^2.

Preliminary Raman frequency measurements for (100) single-crystal silicon strip with (110) applied unidirectional stress are presented in Figure 5. This sample and its stress orientation correspond to
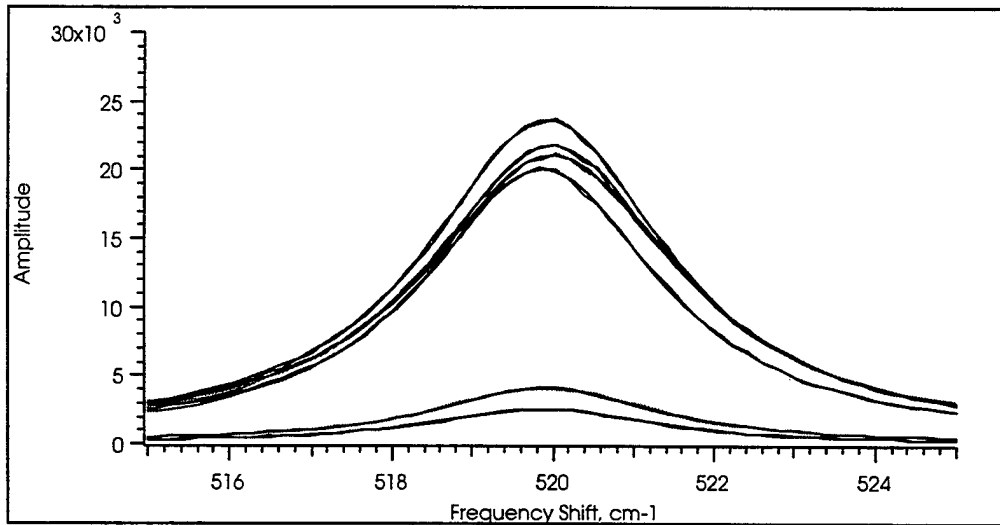

Figure 3.　Raman plot for unstressed single-crystal Si. The various curves represent single spectra sampled at different locations on the wafer. The two lower amplitude cases were obtained without refocusing.
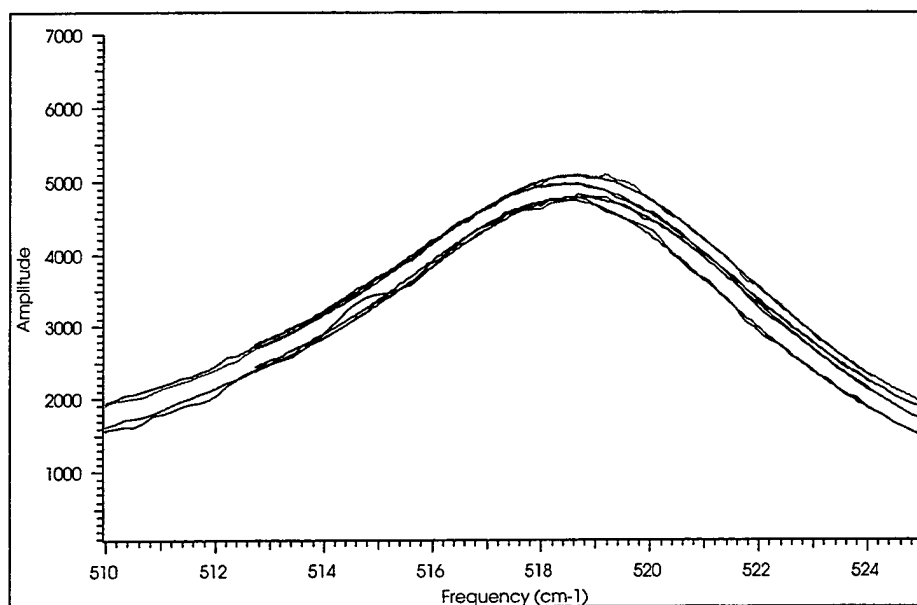
Figure 4.   Raman plot for polysilicon deposited on SiO_2 on single-crystal Si.
Again, the various curves are spectra obtained at different, but
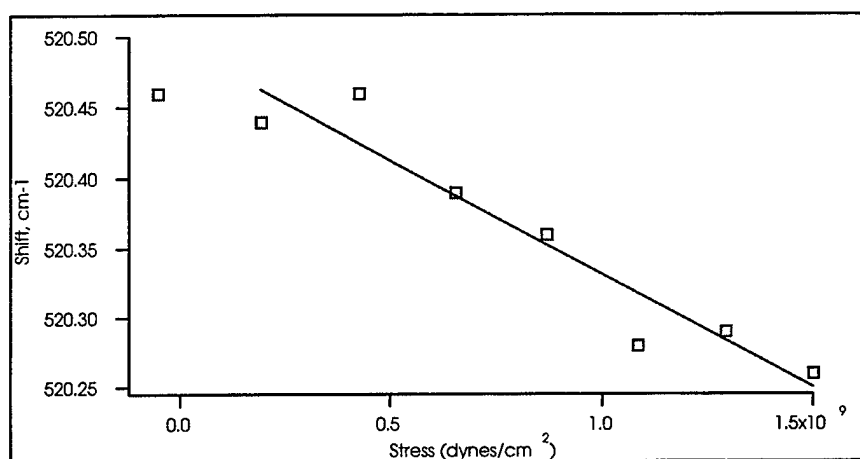randomly located, positions on the wafer.

Figure 5.   Frequency shift as a function of applied stress in the (110) direction. The
sample is a strip of (001) single-crystal silicon. The fitted line has a slope
of -1.62×10^{-10} with an error of 0.23×10^{-10}

the equal biaxial case discussed above. [However the stress plotted in Figure 4 is twice that for the
biaxial case above.] The measured slope is $-1.66 \pm 0.23 \times 10^{-10}$(cm/dyne) compared to the expected
value of 2.0×10^{-10}. The agreement is within 20% of theory. The site from which spectra were
measured is approximately 0.001 in. in size. Spatial variation effects (errors) are expected to be
much smaller than 0.06 cm^{-1}. Additional error due to calibration error of the load cell is estimated to
contribute a 10% error in the stress estimation. The Raman frequency measurements with (100)
applied unidirectional stress are presented in Figure 6. The measured slope is -7.95×10^{-11}. The
theoretical slope is -7.68×10^{-11}. The agreement is well within experimental errors. Again, measure-
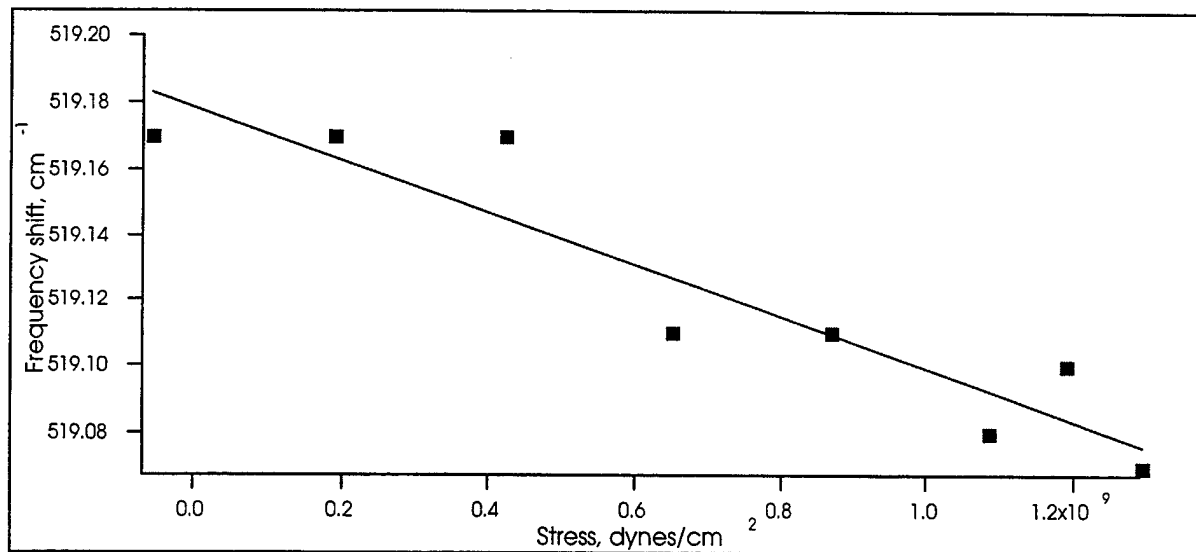
15

Figure 6.   Frequency shift as a function of applied stress in the (100) direction. The sample is a strip of (001) single crystal silicon. The fitted line has a slope of -7.95×10^{-11} with an error of 0.125×10^{-11}.

ments were performed at a single location within a spot of 0.001 in. Deviation from the fitted line is well within 0.002 cm^{-1}, probably representing spatial variations. An estimated 10% error in stress is due to a calibration error on the load cell. Further work to refine the measurements and reduce experimental uncertainties is in progress. This type of data provides the necessary calibration and confirmation of the theoretical and experimental approach taken in this report.

5. Conclusions and Discussion

We have demonstrated analytically that the two-dimensional surface stresses normal to the <001> plane of a cubic crystal have a unique relationship with the Raman frequency shifts. In other words, once the Raman frequency shifts of a cubic crystal (of which its spring constants p, q, r are known) are measured, then the three associated surface-stress components can be uniquely determined. We have also demonstrated that the Raman frequency shifts measured by the use of our in-house system under uni-directional stress in both (110) and (100) directions agree with analytical predictions.

It is to be noted that values of p, q, and r for single-crystal silicon were used in all the calculations. The values for polysilicon may vary from values of single-crystal silicon and may need to be calibrated. In fact, because polysilicon tends to be isotropic in microstructure, there may only be two constants needed to describe the Raman behavior, such as the two Lame elastic constants for an isotropic material. An experimental exercise is required to address this issue. Many investigators have used the p, q, and r values of single-crystal silicon for polysilicon. They also assumed incorrectly that the stress is equal biaxial in the vicinity of discontinuities such as structures. For the backscattered mode used in many of these studies, it is not possible to observe the effect of shear stress on the Raman spectra. Shear stress is expected in the vicinity of long-aspect-ratio structures typically used in microelectronics.

At present, our Raman system uses only backscattered light, which is sensitive to only one of the three possible frequency shifts. More than one observation geometry and polarization condition is required to detect other modes or solutions to Eq. (2).[4,5]

6. Recommendations

Since Raman spectroscopy can provide very localized stress measurements for mini to micro-systems such as microelectronics and MEMS systems, it has a strong potential as an aid in the establishment of reliability assessment techniques. However, although its application to single-crystal systems is well understood, there is a need to expand our understanding to polycrystal systems. It is, therefore, recommended that the Raman technique in stress assessment for polycrystal systems such as polysilicon be investigated.

7. References

1. E. Anastassakis, A. Pinczuk, and E. Burstein, "Effect of Static Uniaxial Stress on the Raman Spectrum of Silicon," *Sol. State Comm.* **88**, Nos. 11/12, pp. 1053-1058, 1993.

2. J. G. Hernandez, and R. Tsu, "Determination of Film-Substrate Microadhesion for Crystalline Silicon Films by Raman Scattering," *Sol. State Comm.* **69**, No. 6, pp. 637-640, 1989.

3. MUMPS or Multi-User MEMS Processes at the MEMS Technology Application Center, MCNC, 3021 Cornwallis Rd, Research Triangle Park, NC 27709.

4. I. De Wolf, "Micro-Raman spectroscopy to study local mechanical stress in silicon integrated circuits," *Semicond. Sci. Technol.* **11**, pp. 139-154(1996) and I. De Wolf, H. E. Maes, and S. K. Jones, "Stress measurements in silicon devices through Raman spectroscopy: Bridging the gap between theory and experiment," *J. Appl. Phys.* **79**, pp. 7148-7156, 1996.

5. R. Loudon, "Raman Effect in Crystals," *Adv. Phys.* **13**, pp. 423-482, 1964.

LABORATORY OPERATIONS

The Aerospace Corporation functions as an "architect-engineer" for national security programs, specializing in advanced military space systems. The Corporation's Laboratory Operations supports the effective and timely development and operation of national security systems through scientific research and the application of advanced technology. Vital to the success of the Corporation is the technical staff's wide-ranging expertise and its ability to stay abreast of new technological developments and program support issues associated with rapidly evolving space systems. Contributing capabilities are provided by these individual organizations:

Electronics and Photonics Laboratory: Microelectronics, VLSI reliability, failure analysis, solid-state device physics, compound semiconductors, radiation effects, infrared and CCD detector devices, data storage and display technologies; lasers and electro-optics, solid state laser design, micro-optics, optical communications, and fiber optic sensors; atomic frequency standards, applied laser spectroscopy, laser chemistry, atmospheric propagation and beam control, LIDAR/LADAR remote sensing; solar cell and array testing and evaluation, battery electrochemistry, battery testing and evaluation.

Space Materials Laboratory: Evaluation and characterizations of new materials and processing techniques: metals, alloys, ceramics, polymers, thin films, and composites; development of advanced deposition processes; nondestructive evaluation, component failure analysis and reliability; structural mechanics, fracture mechanics, and stress corrosion; analysis and evaluation of materials at cryogenic and elevated temperatures; launch vehicle fluid mechanics, heat transfer and flight dynamics; aerothermodynamics; chemical and electric propulsion; environmental chemistry; combustion processes; space environment effects on materials, hardening and vulnerability assessment; contamination, thermal and structural control; lubrication and surface phenomena.

Space Science Application Laboratory: Magnetospheric, auroral and cosmic ray physics, wave-particle interactions, magnetospheric plasma waves; atmospheric and ionospheric physics, density and composition of the upper atmosphere, remote sensing using atmospheric radiation; solar physics, infrared astronomy, infrared signature analysis; infrared surveillance, imaging, remote sensing, and hyperspectral imaging; effects of solar activity, magnetic storms and nuclear explosions on the Earth's atmosphere, ionosphere and magnetosphere; effects of electromagnetic and particulate radiations on space systems; space instrumentation, design fabrication and test; environmental chemistry, trace detection; atmospheric chemical reactions, atmospheric optics, light scattering, state-specific chemical reactions and radiative signatures of missile plumes.

Center for Microtechnology: Microelectromechanical systems (MEMS) for space applications; assessment of microtechnology space applications; laser micromachining; laser-surface physical and chemical interactions; micropropulsion; micro- and nanosatellite mission analysis; intelligent microinstruments for monitoring space and launch system environments.

Office of Spectral Applications: Multispectral and hyperspectral sensor development; data analysis and algorithm development; applications of multispectral and hyperspectral imagery to defense, civil space, commercial, and environmental missions.